Pressure tuning of the Berry phase in $BaMnSb_2$

X. Yin,[1] J. Y. Liu,[2] T. Hu,[3] Y. L. Huang,[1] C. Jiang,[1] L. J. Min,[4] P. G. Li,[5] Z. Q. Mao,[6,2] and H. Xiao[1,*]

[1]*Center for High Pressure Science and Technology Advanced Research, Beijing 100094, China*

[2]*Department of Physics and Engineering Physics, Tulane University, New Orleans, Louisiana 70118, USA*

[3]*Beijing Academy of Quantum Information Science, Beijing 100193, China*

[4]*Department of Materials Science and Engineering, Pennsylvania State University, Pennsylvania 16802, USA*

[5]*Beijing University of Posts and Telecommunications, Beijing 100876, China*

[6]*Department of Physics, Pennsylvania State University, Pennsylvania 16802, USA*

(Received 31 August 2021; accepted 4 January 2022; published 18 January 2022)

The Sb square net in $BaMnSb_2$ is reported to host nearly massless Dirac fermions. At ambient pressure, $BaMnSb_2$ shows strong Shubnikov–de Haas (SdH) oscillations with a π Berry phase. In this work, we study $BaMnSb_2$ under different pressures. It is found that the frequency of the SdH oscillation remains almost unchanged, hence the cross-section area of the Fermi surface does not change much with pressure. Notably, there is a sudden change in the phase factor of the oscillations around a critical pressure of $P = 2.5$ GPa, which suggests a possible topological phase transition in $BaMnSb_2$.

DOI: 10.1103/PhysRevB.105.045123

I. INTRODUCTION

One of the key concepts in condensed matter physics is the classification of distinctive phases of matter. In the past, quantum states are classified by the principle of spontaneous symmetry breaking. A completely different view based on the concept of topological order, arises after the discovery of the quantum Hall state [1–3]. The topological order parameters for topological quantum states play the role of conventional symmetry-breaking order parameters. Topological insulators, which have a bulk band gap like an ordinary insulator, with protected conducting states on their edges or surfaces, have attracted great interest and become a rapidly developing field. Surface states in theses materials can be described by the Dirac equation with the Fermi surface formed by Dirac bands. Exotic states, such as the novel quantum Hall state [4] and Majorana fermions [5] can occur at the surface of a topological insulator. In addition to their fundamental interest, these materials are also useful for applications such as spintronics devices and quantum computation.

Topological semimetals are states of quantum matter, which are different from topological insulators and are characterized by the topological stability of the Fermi surface, whether it encloses band crossing points [6]. It hosts either Dirac fermions or Weyl fermions. Dirac fermions are protected by both time reversal symmetry and crystalline inversion symmetry. Dirac semimetals evolve into Weyl semimentals when either of them is broken. Weyl semimetals due to broken inversion symmetry was first realized in TaAs-class materials [7]. The other way to obtain the Weyl phase is to break the time reversal symmetry by introducing magnetic ordering. Thus, magnetic compounds with Dirac type band crossing are promising candidates for hosting Weyl fermions [8]. The layered compound $XMnBn_2$ (X = Ca, Sr, Ba, Bn = Bi or Sb) is characterized as either three-dimensional Dirac or Weyl semimetals [9–14]. The two- dimensional (2D) Bi square net hosts massive Dirac electrons due to a significantly large spin orbital coupling effect, making it hard to observe interesting phenomena related to massless Dirac fermions, while the Sb square net is reported to host nearly massless Dirac fermions [10,15].

$BaMnSb_2$ has a small effective mass ($\sim$0.052 m_0) among the $XMnBn_2$ family and possesses a small Fermi surface with the most significant 2D character [10,15,16]. Previously it is reported that $BaMnSb_2$ crystallizes in a tetragonal structure ($I4/mmm$) [10,15,17,18], with $a = b = 4.556$ Å and $c = 24.299$ Å [15]. However, recent single-crystal x-ray structural analysis, scanning transmission electron microscopy, neutron scattering, and optical second harmonic generation measurements, found that $BaMnSb_2$ involves weak orthorhombic distortion, which is hard to be resolved [16,19]. $BaMnSb_2$ actually possesses a noncentrosymmetric orthorhombic structure where the Sb square net is distorted to a zigzag chainlike structure (space group $I2mm$), with $a = 4.4583$ Å, $b = 24.2161$ Å, and $c = 4.5141$ Å [19].

The structure of $BaMnSb_2$ consists of an alternating stack of a 2D Dirac fermion conduction layer and a insulating layer [20]. The distorted square net has great influence on the electronic states and opens a sizable gap at the Dirac points on the $\Gamma - M$ lines [19]; while for similar compounds with tetragonal structure, the Dirac-like bands along the $\Gamma - M$ line crosses the Fermi energy, forming four equivalent valleys [9,14,20]. The interplay among inversion symmetry breaking, spin orbital coupling (SOC) and valley degree of freedom in $BaMnSb_2$ results in a unique electronic state with spin-valley locking [16,19]. In addition, well-defined Hall plateaus accompanied by vanishing conductivity at high fields

*hong.xiao@hpstar.ac.cn

reveals three-dimensional (3D) quantum Hall effect [16]. A quantum liquid-2D chiral surface state is also reported to be present in the system [16]. Furthermore, theoretical calculations found that in $BaMnSb_2$, the nonzero local Berry curvature of electrons can induce a phonon angular momentum, and the direction of the phonon angular momentum is locked to the phonon propagation direction, i.e., "phonon helicity", analogous to electron helicity in spin-orbit coupled electronic systems [21].

$BaMnSb_2$ provides a good candidate for investigation of novel exotic phenomena of massless Dirac fermions. The nontrivial Berry phase, small cyclotron mass and high carrier mobility suggest that Dirac band crossing points may be closer to the Fermi level in $BaMnSb_2$ [10]. High pressure provides a clean and effective way to tune the lattice parameter and drastically impact the electronic structure [22–24]. In this work, we study the Shubnikov–de Haas (SdH) oscillations of $BaMnSb_2$ under high pressures. The frequency of the SdH oscillations remains almost unchanged, which suggests that the cross-section area of the Fermi surface does not change much with pressure. Notably, there is a sudden change in the Berry phase factor at about 2.5 GPa, possibly associated with a topological phase transition. Thus, although pressure has no obvious effect on the Fermi level in the investigated pressure range, the SOC induced gap near the Dirac nodes may be closed and becomes topological trivial with pressure tuning.

II. EXPERIMENTAL DETAILS

High quality single crystals of $BaMnSb_2$ were synthesized using a self-flux method [10]. Electrical resistivity was measured using a Quantum Design Physical Property Measurement System (PPMS). We use a van der Pauw method to measure the resistivity and the Hall resistivity simultaneously [25]. Pressure was applied at room temperature using diamond anvil cells (DAC) made of CuBe alloy, with the diamond anvil culet of 800 μm in diameter. Pressure was calibrated by using the ruby fluorescence shift at room temperature. The sample is sanded and the thickness of the sample loaded in the DAC is about 30 μm.

III. RESULTS AND DISCUSSION

The resistivity and Hall resistivity of $BaMnSb_2$ were measured simultaneously under different applied pressures. Figures 1(a)–1(f) shows the magnetic field B dependence of the resistivity ρ_{xx} at pressure $P = 0.93$, 1.64, 2.2, 2.68, 3.24, 3.64, and 4.12 GPa, respectively. At each pressure, the measurements were performed under different temperatures. Strong Shubnikov–de Haas (SdH) oscillations are observed in the resistivity data. With increasing pressure, the oscillation becomes weaker. Figures 2(a)–2(f) plots the B dependence of the Hall resistivity ρ_{xy} under different applied pressures. It is found that ρ_{xy} linearly depends on B up to the highest magnetic field, with additional features of oscillation. The slope of the linear curve is positive, suggesting that the dominated charge carrier is hole, which is the same as $BaMnSb_2$ at ambient condition [10,15]. The linear field dependence of the ρ_{xy} is also observed in $SrMnSb_2$ at $T = 2$ K. For $CaMnSb_2$, ρ_{xy} exhibits linear field dependence at high temperature, while

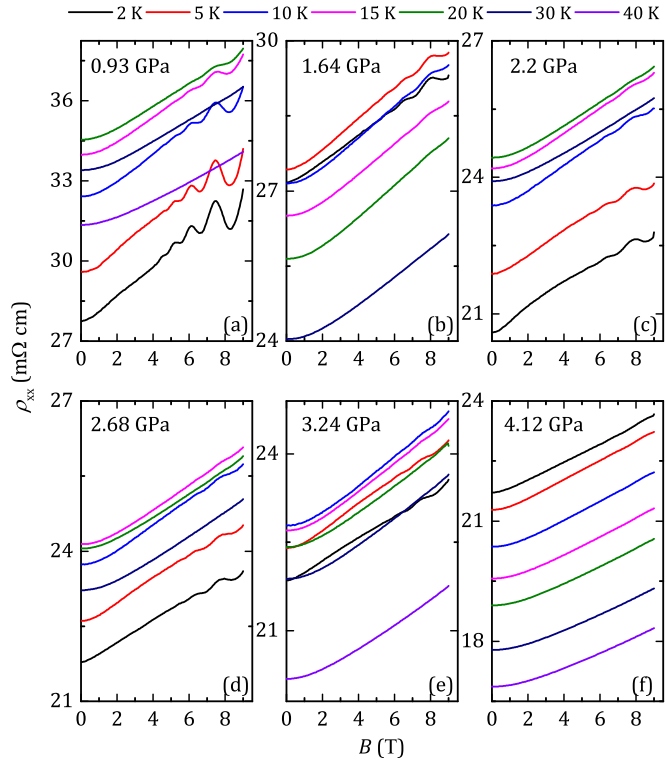

FIG. 1. (a)–(f) Magnetic field B dependence of the resistivity ρ_{xx} at different applied pressures, $P = 0.93$, 1.64, 2.2, 2.68, 3.24, and 4.12 GPa.

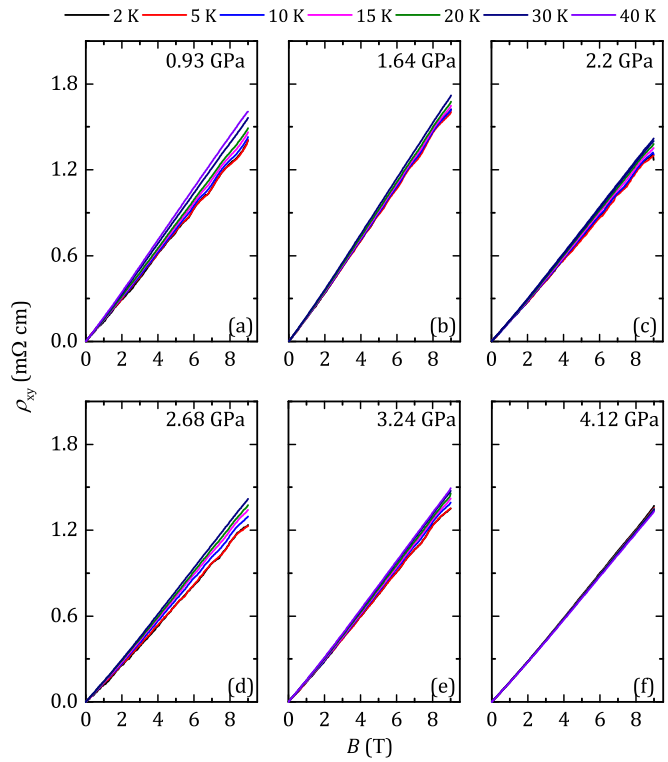

FIG. 2. (a)–(f) Magnetic field B dependence of the Hall resistivity ρ_{xy} at different applied pressures, $P = 0.93$, 1.64, 2.2, 2.68, 3.24, and 4.12 GPa.

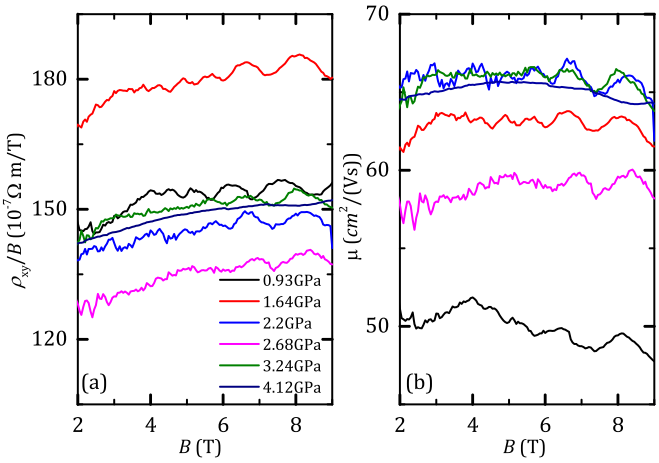

FIG. 3. (a) The magnetic field B dependence of ρ_{xy}/B at $T = 2$ K under different pressures, $P = 0.93$, 1.64, 2.2, 2.68, 3.24, and 4.12 GPa. (b) The H dependence of the transport mobility μ at $T = 2$ K under different pressures, $P = 0.93$, 1.64, 2.2, 2.68, 3.24, and 4.12 GPa.

at low temperatures, ρ_{xy} shows obvious downward curvature, suggesting that $CaMnSb_2$ is a multicarrier system [26]. The B dependence of ρ_{xy}/B at $T = 2$ K under different pressures are plotted in Fig. 3(a) and ρ_{xy}/B is weakly B dependent. The B dependence of the transport mobility $\mu = \frac{\rho_{xy}}{\rho_{xx}B}$ (Ref. [27]) under different pressures is shown in Fig. 3(b).

We extracted the oscillatory component of the resistivity $\Delta\rho_{xx}$ vs $1/B$ at $P = 0.93$, 1.64, 2.2, 2.68, 3.24, and 4.12 GPa, as shown in Figs. 4(a)–4(f). The Landau level (LL) fan diagram at the corresponding pressures is plotted in Figs. 4(g)–4(l), which is constructed from the SdH oscillations of ρ_{xx}. When the Landau quantization of the energy states occurs in magnetic fields, the density of states (DOS) becomes periodically modulated which results in the oscillation phenomena [28]. The phase shift of SdH oscillation provides a way to quantitatively characterize the Berry phase accumulated in cyclotron orbits of the system [29]. If a quantum system undergoes adiabatic changes and the Hamiltonian returned to its original form, the system will return to its original state, apart from an additional phase factor, i.e., Berry's phase [29,30]. With the Brillouin zone playing the role of the parameter space, Berry's theory are applicable to an electron moving in a crystal and Berry's phase can be used for labeling energy bands in solids [30,31]. In SdH oscillations, conductivity oscillates periodically as a function of $1/B$. The oscillatory part of the conductivity σ_{xx} follows $\Delta\sigma_{xx} \approx \cos[2\pi(\frac{F}{B} - \frac{1}{2} + \beta)]$, where F is the oscillation frequency and β is the phase shift. In crystals the semiclassical quantization condition for energy levels of electrons in the magnetic field depends on Berry's phase [30,32]: $A_N = \frac{2\pi e}{\hbar}B(N + \frac{1}{2} - \beta)$, where $\beta = \frac{\gamma}{2\pi}$, γ is the Berry phase, A_N is the external area enclosed by electrons in the $k-$space with their cyclotron orbits on the Fermi surface. Note that for Dirac fermions possessing a linear energy dispersion $\gamma = \pi(\beta = \frac{1}{2})$; $\gamma = 0$ ($\beta = 0$) for a parabolic energy dispersion. When the Fermi energy E_F lies in between two neighboring LLs, the DOS takes a minimum; when the Fermi energy E_F lies at the center of a LL, DOS takes a maximum. The minimum in σ_{xx} occurs when DOS takes a minimum (a complete filling of some N LLs). Thus, the

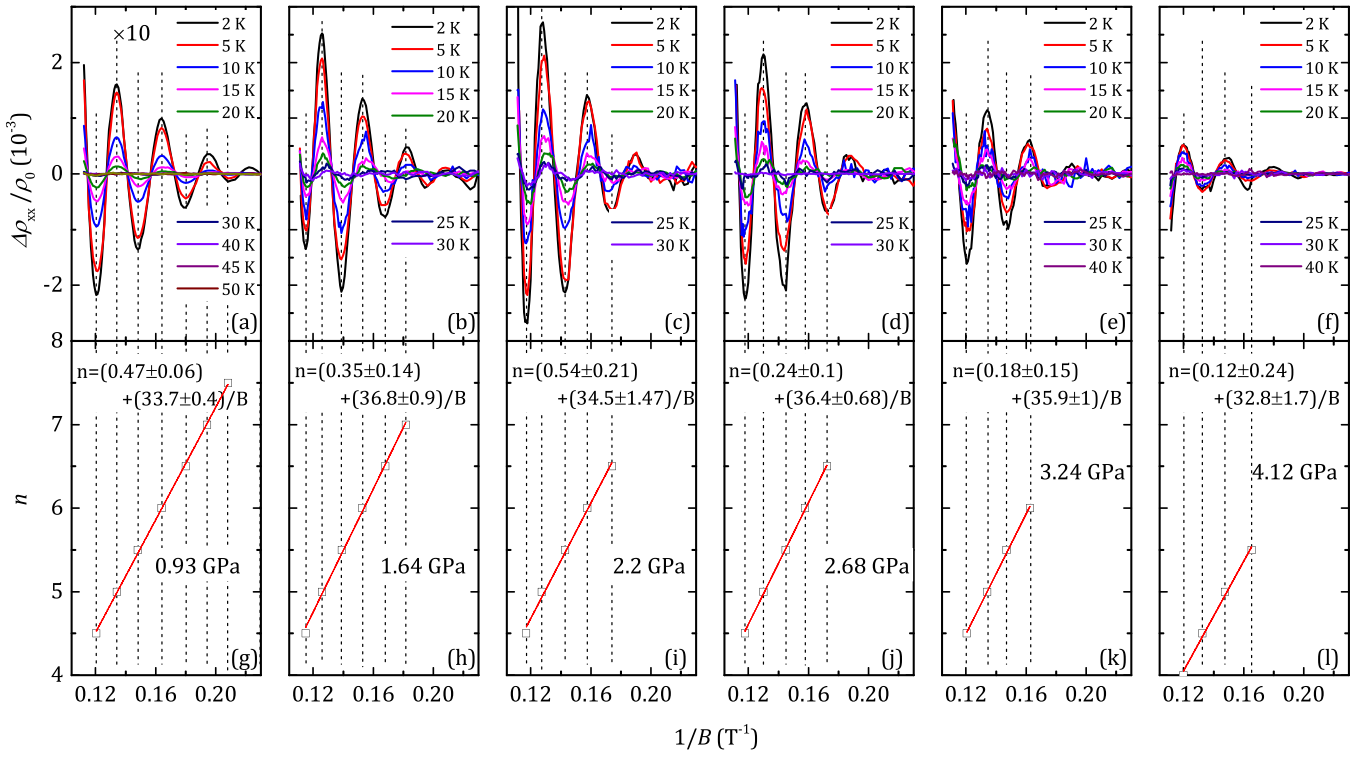

FIG. 4. (a)–(f) The oscillatory component of the resistivity $\Delta\rho_{xx}$ vs $1/B$ at $P = 0.93$, 1.64, 2.2, 2.68, 3.24, and 4.12 GPa, respectively. (g)–(l) LL fan diagram at corresponding pressures. The solid lines represent the linear fits.

integer index N should be assigned to that minimum of σ_{xx} and the phase factor β in the SdH oscillations can be determined from the analysis of the LL fan diagram [28,30,32].

Since ρ_{xx} and ρ_{xy} instead of σ_{xx} are obtained in experiments, it is more convenient to use ρ_{xx} for indexing the integer n. In-plane conductivity σ_{xx} can be converted from the longitudinal resistivity ρ_{xx} and the transverse resistivity ρ_{xy} using $\sigma_{xx} = \rho_{xx}/(\rho_{xx}^2 + \rho_{xy}^2)$ [33]. The minimum in σ_{xx} could correspond to either maxima or minima in $\Delta\rho_{xx}$, which is dependent on the ratio of ρ_{xx}/ρ_{xy}. We list some literature to show how the integer n is determined by the minimum or maximum of ρ_{xx} depending on the ratio of ρ_{xx}/ρ_{xy}. When ρ_{xx} is smaller than ρ_{xy}, the minimum of ρ_{xx} is used for indexing the integer n [16,34]; when ρ_{xx} is larger than ρ_{xy}, the maximum of ρ_{xx} is used for indexing the integer n, for example, Ref. [33], where $|\rho_{xx}/\rho_{xy}| = 17.5$ at 2 K and 9 T and Ref. [10], where ρ_{xy} is about 1/4–1/3 ρ_{xx}. In our case, ρ_{xy} is at least 10 times smaller than ρ_{xx}, thus $\sigma_{xx} \approx 1/\rho_{xx}$ and the integer LL indices are assigned to the maxima of ρ_{xx} [10,15]. In particular, $BaMnSb_2$ samples were investigated before, which showed either $\rho_{xx}/\rho_{xy} < 1$ or $\rho_{xx}/\rho_{xy} > 1$ for different doping [16]. For pure and Eu doped $BaMnSb_2$ (Ref. [16], sample B#1 and E#1 in Figs. 3 and 4, respectively), $\rho_{xx}/\rho_{xy} < 1$ and the minimum of ρ_{xx} is used to indexing the integer n. On the other hand, for $BaMnSb_2$ with Zn doping (Ref. [16], Supplemental Material Fig. 4, sample Z#1), $\rho_{xx}/\rho_{xy} > 1$ and the ρ_{xx} peaks are located, e.g., at $B = 3.47$ and 5.79 T, roughly. The integer n is located at $B_F/B = 1.5$ and 2.5 (Ref. [16], Supplemental Material Fig. 4), with $B_F = 8.9$ T (Ref. [16], Supplemental Material Table 2), thus the corresponding $B = 8.9/1.5 = 5.93$ and $B = 8.9/2.5 = 3.56$, consistent with the peak position in ρ_{xx}. Thus the maximum of ρ_{xx} is used to indexing the integer n, which is in agreement with Berry phase determination in our work. The solid lines in the LL fan diagram [Figs. 4(g)–4(l)] are fitting curves. The slope of the linear fitting reflects the frequency F and the intercept on the LL index axis obtained from the extrapolation of the linear fit in the fan diagram is the Berry phase factor.

Figure 5(a) shows the temperature dependence of the fast Fourier transformation (FFT) analyses of $\Delta\rho_{xx}$ at different temperatures under an applied pressure of $P = 0.93$ GPa. It is found that the SdH oscillations of ρ_{xx} consists of a single frequency which is 32.6 T. This suggests that the oscillations result from a single band, which is consistent with the low T data at ambient condition in both SdH [8,10,15] and de Haas–van Alphen results [8]. Figure 5(b) plots the normalized FFT amplitude at different pressures. The open symbols represent the data obtained from the FFT analyses; the solid symbols are data taken directly from the peak positions. For $P = 0.93$ GPa, both methods are applied and the data are consistent. The effective cyclotron mass m^* can be extracted from the fit of the temperature dependence of the normalized FFT peak amplitude to the thermal damping factor of Lifshitz-Kosevich equation, i.e.,

$$\Delta\rho/\rho_0 \propto \exp(-\alpha T_D \mu/B) * \alpha T\mu / \left[\bar{B} * \sinh\left(\frac{\alpha T \mu}{\bar{B}}\right)\right]$$

where, ρ_0 is the zero field resistivity, $\alpha = (2\pi^2 k_B m_0)/(\hbar e)$, $T_D = \hbar/(2\pi k_B \tau_q)$ is the Dingle temperature, μ is the ratio

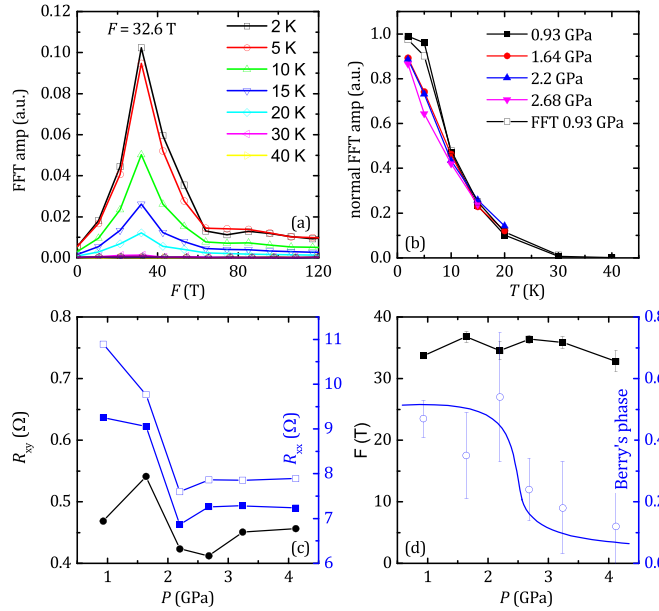

FIG. 5. (a) The FFT amplitude vs frequency for $P = 0.93$ GPa at different temperatures. (b) The normalized FFT amplitude vs temperature for different pressures. (c) The pressure dependence of the resistance R_{xx} and Hall resistance R_{xy} at $T = 2$ K. Open squares and solid circles represent data at $B = 9$ T, solid squares are data for $B = 0$ T. (d) The pressure dependence of the extracted phase factor and the frequency of the SdH oscillation.

of effective mass of cyclotron motion to the free electron mass, $1/\bar{B}$ is the average inverse field for FFT analysis. For $P = 0.93$ GPa, the best fits give $m^* = 0.13\ m_e$. The quantum mobility μ_q is related with the quantum relaxation time, i.e., $\mu_q = e\tau_q/m^*$, where τ_q is the quantum life time. μ_q is estimated to be 50 $cm^2V^{-1}s^{-1}$. This value is consistent with the transport mobility obtained from the Hall coefficient and resistivity data, μ_{tr} is also about 50 $cm^2/V^{-1}s^{-1}$ at $T = 2$ K and $P = 0.93$ GPa. Based on the plot, the data normalized at 2 K almost overlap each other. Hence the effective mass and quantum mobility does not change much in the applied pressure range.

The resistance R_{xx} at $T = 2$ K with $B = 0$ and $B = 9$ T, and Hall resistance R_{xy} at $T = 2$ K with $B = 9$ T as a function of pressure are summarized in Fig. 5(c). It is found that all of them shows a sudden decrease around 2.2 GPa and tends to saturate with further increasing pressure. Figure 5(d) plots the pressure dependence of the frequency (solid squares) and the Berry's phase. It seems that the Berry's phase shows a sudden drop at a critical pressure between 2.2 and 2.68 GPa and it tends to be close to zero at high pressures. However, since the oscillation amplitude is small at high pressures, the uncertainty in determining the phase increases. The sudden change in the pressure dependence of R_{xx} and R_{xy} around the same pressure seems to be consistent with the phase change. Nevertheless, further study under high magnetic fields will be helpful to determine the Berry phase more accurately. The sudden change in the Berry phase suggests a possible topological phase transition in $BaMnSb_2$.

Note that the pressure induced change in Berry phase is previously reported in Dirac semimetal Cd_3As_2, where a

sudden change in the phase factor of the oscillations occurs at $P = 1.3$ GPa [35]. The topological phase transition in Cd_3As_2 is not coincident with the structural phase transition which happens at higher pressure of about 2.5 GPa [35]. The change in the phase factor was attributed to pressure-driven annihilation of Dirac nodes and opening of a band gap: with increasing pressure, the c/a ratio decreases and the Dirac nodes shift closer to the Brillouin zone center, and eventually the time-reversed Dirac partners annihilate and a band gap around 20 meV opens up [33,35].

A similar topological phase transition is observed in ZrSiS. SdH measurements on the topological nodal line semimetal ZrSiS which hosts multiple Dirac cones found two distinct oscillation frequencies and the smaller orbit shows a possible pressure-induced topological quantum phase transition at a pressure between 0.16 and 0.5 GPa, which is accompanied by an abrupt decrease of the cross-sectional area of the Fermi surface below 0.5 GPa and then increases at higher pressure [33]. Similar to Cd_3As_2, the change in the phase factor in ZrSiS is not due to a structural change [33,35]. The possibilities are excluded that the phase change is associated with magnetic field dependence/chemical potential position dependence of the phase factor or Zeeman splitting which would complicate the determination of the phase factor [33]. The changes are consistent with a pressure-driven topological quantum phase transition in which a bulk band gap is introduced [33].

In $BaMnSb_2$, density functional theory calculations show that the DOS near the Fermi level is mainly contributed by the p orbital of the Sb atoms which induces the Dirac related band structure [16,17]. Two gapped Dirac cones near the Fermi energy emerge at two different momenta $K_{\pm}$, located symmetrically around the X point along the X-M line [16]. Based on present data and also previous reports [10,15], the effective mass of the Dirac fermion is small and the Hall coefficient is positive, thus it seems that the crossing point of the linear Dirac band crossing is located right above the Fermi level, i.e., the Fermi pocket hosting Dirac Fermions should be a hole pocket and small, which has been observed in angular-resolved photoemission spectroscopy measurements [16]. With pressure tuning, the Fermi level and the hole pockets which host the Dirac Fermions remain almost unchanged, since the Hall coefficient is always positive and the frequency of the oscillation changes little with pressure. Previous first principles calculations have predicted that the SOC induced gap near the Dirac node is as small as ∼20 meV [16]. Thus, the small gap could be easily tuned: it closes under pressure and the band structure becomes topological trivial with further increasing pressure. There is also a possibility that the two spin-valley locked Dirac cones at K+ and K- annihilate when the pressure is increased above 2.2 GPa, thus creating a trivial hole pocket at the X point.

Notably, although modest pressure is required to tune the electronic state in materials like $BaMnSb_2$, Cd_3As_2, and ZrSiS, where the topological phase transition is observed at ∼2.5, ∼1.3, and ∼0.5 GPa, respectively, for other topological semimetals, such as the noncentrosymmetric NbAs-type transition-metal monoarsenides with 12 pairs of Weyl nodes in their 3D Brillouin zones [7,36–38], the Fermi surface and band structure may not be easily tuned by external pressures over a moderate range. The large Debye temperature Θ_D of NbAs is 450 K, indicating that the crystalline lattice is robust under pressure [38].

IV. CONCLUSIONS

Transport measurements were performed on a $BaMnSb_2$ single crystal sample under different applied pressures. It shows strong SdH oscillations initially and eventually disappear with further increasing pressure. Hall effect measurements found that the dominant charge carrier is hole and the slope of the linear ρ_{xy} vs B curve does not change much with pressure. The area of the Fermi surface remains almost unchanged with pressure, but there is a sudden change in the Berry phase factor, suggesting a possible topological phase transition.

ACKNOWLEDGMENTS

We thank H. Y. Xie from Beijing Academy of Quantum Information Science (BAQIS) for insightful discussions. Work at HPSTAR was supported by NSAF, Grant No. U1530402. Work at BAQIS was supported by NSFC, Grant No. 11574338. Z.Q.M. acknowledges the support from the U.S. National Science Foundation under Grant No. DMR1917579.

[1] M. Z. Hasan and C. L. Kane, Rev. Mod. Phys. **82**, 3045 (2010).
[2] A. Bansil, H. Lin, and T. Das, Rev. Mod. Phys. **88**, 021004 (2016).
[3] X.-L. Qi and S.-C. Zhang, Rev. Mod. Phys. **83**, 1057 (2011).
[4] Y. Zheng and T. Ando, Phys. Rev. B **65**, 245420 (2002).
[5] L. Fu and C. L. Kane, Phys. Rev. Lett. **100**, 096407 (2008).
[6] H. Weng, X. Dai, and Z. Fang, J. Phys.: Condens. Matter **28**, 303001 (2016).
[7] Y. Zhou, P. Lu, Y. Du, X. Zhu, G. Zhang, R. Zhang, D. Shao, X. Chen, X. Wang, M. Tian, J. Sun, X. Wan, Z. Yang, W. Yang, Y. Zhang, and D. Xing, Phys. Rev. Lett. **117**, 146402 (2016).
[8] S. Huang, L. Xing, R. Chapai, R. Nepal, and R. Jin, Phys. Rev. Mater. **4**, 065001 (2020).
[9] S. Borisenko, D. Evtushinsky, Q. Gibson, A. Yaresko, K. Koepernik, T. Kim, M. Ali, J. van den Brink, M. Hoesch, A. Fedorov, E. Haubold, Y. Kushnirenko, I. Soldatov, R. Schäfer, and R. J. Cava, Nat. Commun. **10**, 3424 (2019).
[10] J. Liu, J. Hu, H. Cao, Y. Zhu, A. Chuang, D. Graf, D. J. Adams, S. M. A. Radmanesh, L. Spinu, I. Chiorescu, and Z. Mao, Sci. Rep. **6**, 30525 (2016).
[11] L.-L. Jia, Z.-H. Liu, Y.-P. Cai, T. Qian, X.-P. Wang, H. Miao, P. Richard, Y.-G. Zhao, Y. Li, D.-M. Wang, J.-B. He, M. Shi, G.-F. Chen, H. Ding, and S.-C. Wang, Phys. Rev. B **90**, 035133 (2014).
[12] K. Wang, D. Graf, L. Wang, H. Lei, S. W. Tozer, and C. Petrovic, Phys. Rev. B **85**, 041101(R) (2012).

[13] K. Wang, D. Graf, H. Lei, S. W. Tozer, and C. Petrovic, Phys. Rev. B **84**, 220401(R) (2011).
[14] J. Park, G. Lee, F. Wolff-Fabris, Y. Y. Koh, M. J. Eom, Y. K. Kim, M. A. Farhan, Y. J. Jo, C. Kim, J. H. Shim, and J. S. Kim, Phys. Rev. Lett. **107**, 126402 (2011).
[15] S. Huang, J. Kim, W. A. Shelton, E. W. Plummer, and R. Jin, Proc. Natl. Acad. Sci. **114**, 6256 (2017).
[16] J. Y. Liu, J. Yu, J. L. Ning, H. M. Yi, L. Miao, L. J. Min, Y. F. Zhao, W. Ning, K. A. Lopez, Y. L. Zhu, T. Pillsbury, Y. B. Zhang, Y. Wang, J. Hu, H. B. Cao, B. C. Chakoumakos, F. Balakirev, F. Weickert, M. Jaime, Y. Lai *et al.*, Nat. Commun. **12**, 4062 (2021).
[17] M. A. Farhan, G. Lee, and J. H. Shim, J. Phys.: Condens. Matter **26**, 042201 (2014).
[18] G. Cordier and H. Schäfer, Z. Naturforsch. B **32**, 383 (1977).
[19] H. Sakai, H. Fujimura, S. Sakuragi, M. Ochi, R. Kurihara, A. Miyake, M. Tokunaga, T. Kojima, D. Hashizume, T. Muro, K. Kuroda, T. Kondo, T. Kida, M. Hagiwara, K. Kuroki, M. Kondo, K. Tsuruda, H. Murakawa, and N. Hanasaki, Phys. Rev. B **101**, 081104(R) (2020).
[20] G. Lee, M. A. Farhan, J. S. Kim, and J. H. Shim, Phys. Rev. B **87**, 245104 (2013).
[21] L.-H. Hu, J. Yu, I. Garate, and C.-X. Liu, Phys. Rev. Lett. **127**, 125901 (2021).
[22] H.-K. Mao, B. Chen, J. Chen, K. Li, J.-F. Lin, W. Yang, and H. Zheng, Matter Radiat. Extremes **1**, 59 (2016).
[23] H.-K. Mao, X.-J. Chen, Y. Ding, B. Li, and L. Wang, Rev. Mod. Phys. **90**, 015007 (2018).
[24] V. Struzhkin, B. Li, C. Ji, X.-J. Chen, V. Prakapenka, E. Greenberg, I. Troyan, A. Gavriliuk, and H.-k. Mao, Matter Radiat. Extremes **5**, 028201 (2020).
[25] L. J. van der Pauw, Philips Tech. Rev. **20**, 220 (1958).
[26] J. B. He, Y. Fu, L. X. Zhao, H. Liang, D. Chen, Y. M. Leng, X. M. Wang, J. Li, S. Zhang, M. Q. Xue, C. H. Li, P. Zhang, Z. A. Ren, and G. F. Chen, Phys. Rev. B **95**, 045128 (2017).
[27] Y. Xie, C. Bell, M. Kim, H. Inoue, Y. Hikita, and H. Y. Hwang, Solid State Commun. **197**, 25 (2014).
[28] Y. Ando, J. Phys. Soc. Jpn. **82**, 102001 (2013).
[29] M. V. Berry, Proc. R. Soc. London A **392**, 45 (1984).
[30] G. P. Mikitik and Y. V. Sharlai, Phys. Rev. Lett. **82**, 2147 (1999).
[31] J. Zak, Phys. Rev. Lett. **62**, 2747 (1989).
[32] D. Shoenberg, *Magnetic Oscillations in Metals* (Cambridge University Press, Cambridge, 1984).
[33] D. VanGennep, T. A. Paul, C. W. Yerger, S. T. Weir, Y. K. Vohra, and J. J. Hamlin, Phys. Rev. B **99**, 085204 (2019).
[34] H. Masuda, H. Sakai, M. Tokunaga, Y. Yamasaki, A. Miyake, J. Shiogai, S. Nakamura, S. Awaji, A. Tsukazaki, H. Nakao, Y. Murakami, T.-h. Arima, Y. Tokura, and S. Ishiwata, Sci. Adv. **2**, e1501117 (2016).
[35] C. Zhang, J. Sun, F. Liu, A. Narayan, N. Li, X. Yuan, Y. Liu, J. Dai, Y. Long, Y. Uwatoko, J. Shen, S. Sanvito, W. Yang, J. Cheng, and F. Xiu, Phys. Rev. B **96**, 155205 (2017).
[36] R. D. dos Reis, S. C. Wu, Y. Sun, M. O. Ajeesh, C. Shekhar, M. Schmidt, C. Felser, B. Yan, and M. Nicklas, Phys. Rev. B **93**, 205102 (2016).
[37] J. Zhang, F.-L. Liu, J.-K. Dong, Y. Xu, N.-N. Li, W.-G. Yang, and S.-Y. Li, Chin. Phys. Lett. **32**, 097102 (2015).
[38] Y. Luo, N. J. Ghimire, E. D. Bauer, J. D. Thompson, and F. Ronning, J. Phys.: Condens. Matter **28**, 055502 (2015).